

# DCARIESNET: DENTAL CARIES SEGMENTATION WITH THREE-FOLD FEATURES AND OPTIMIZED U-NET

Mohamed Shajahan

Razak Faculty of Technology and Informatics, Universiti Teknologi Malaysia, Kuala Lumpur Campus,  
Malaysia College of Engineering, University of Business and Technology, Jeddah, Saudi Arabia  
mdshajahanh@yahoo.co.in

Sahnus Usman<sup>1</sup>,

<sup>1</sup>Razak Faculty of Technology and Informatics, Universiti Teknologi Malaysia, Kuala Lumpur Campus,  
Malaysia  
Sahnus.kl@utm.my

Siti Armiza Mohd Aris<sup>1</sup>

<sup>1</sup>Razak Faculty of Technology and Informatics, Universiti Teknologi Malaysia, Kuala Lumpur Campus,  
Malaysia  
Armiza.kl@utm.my

Norliza Mohd Noor.<sup>1</sup>

<sup>1</sup>Razak Faculty of Technology and Informatics, Universiti Teknologi Malaysia, Kuala Lumpur Campus,  
Malaysia  
norliza@utm.my

## Abstract

Early detection of dental caries is essential for effective treatment. The refore, deep learning methods have achieved extraordinary radiological diagnostic efficiency. This research seeks to effectively employ the DCariesNet based deep learning approach for dental caries segmentation. The DCariesNet is utilized for identifying dental caries-affected regions in X-ray images. The three main steps of the newly proposed DCariesNet are "(a) Pre-processing, (b) Feature Extraction, and (c) Dental caries Segmentation." The acquired dental X-ray images are first pre-processed using Partition Supported Median, Interpolation, and Discrete Wavelet Transform (NRPMID), morphological operations (dilation, erosion, opening, and closure), and histogram equalization. The three-fold features, like Local Binary Pattern (LBP), Local Discriminative Pattern (LDP), and Local Optimal-Oriented Pattern (LOOP) are extracted from the pre-processed images. To train the segmentation framework, these retrieved characteristics are combined. A novel, improved U-NET-based CNN architecture is used to mimic the dental caries segmentation phase. A novel Aquila Explored Crow search Optimizer (CrAqOA) is used to optimize the weight function of U-NET. The standard Aquila Optimizer (AO) and standard Crow Search Optimization (CSA) concepts are blended to create the CrAqOA model. The segmented result (i.e. caries affected area) is the end outcome of the optimized U-NET. The proposed model assists in the early diagnosis of dental cavities with enhanced accuracy. Finally, to confirm the effectiveness of the anticipated model, a comparison evaluation is conducted.

**Keywords:** Dental Caries; Segmentation; NRPMID; Optimized U-NET; CrAqOA.

## 1. Introduction

Dental caries is described as a localized ailment that damages the hard tissues of the tooth and is brought on by fermentable carbohydrates being consumed by plaque-associated microbes [1]-[4]. It still is a significant public health issue and remains one of the most widespread dental disorders, impacting 60 to 90% of school-aged children [5]-[7]. Caries commonly referred to as oral decay or dental decay [3], can appear on every enamel surface, though it is more common wherever dental plaque is continuously being deposited [9]-[12]. "The ECM, X-rays, FOTI, fluorescent methods, OCT, and ultrasound techniques" are only a slew of professionally available tools for finding caries [5] [13], [3], [14], [15],[16].

As X-rays seem to be accessible and less expensive than other procedures, they are unquestionably the most used approach for identifying caries. Dental professionals frequently employ X-rays for medical diagnostics [6],

and [7]. Dental X-rays are a necessary, therapeutic, and preventive tool that yields useful data. Dental caries radiographic interpretations are always done in conjunction with an oral cavity pathological evaluation. Particularly in the latter stages of the disease whenever the tooth structures have sufficiently undergone decalcification, cavities are detectable radiographically [25]-[27].

When it comes to digitally acquire, manipulating, storing, retrieving, and exchanging radiography information, image processing methods are essential [28], [49]. Since it is still a developing technology, digital image radiography has certain distinct benefits over film-based radiography but also poses new and unique obstacles [29]-[31]. The diagnostic procedure can benefit from the usage of digital image processing tools [32]. Today, automated or even semi-automatic segmentation of digital dental radiographs is frequently utilized for diagnostic purposes, enabling the dentist to quickly diagnose cavities [33]. Recently, a segmentation algorithm for computer-aided caries segmentation was created to make decisions about the diagnosis of caries and subsequent treatment more efficiently and effectively.

The technique of segmentation splits an image into its items or areas. The challenge is handled depending on the amount of granularity at which the subdivision was indeed done. Thus, segmentation comes to an end once the application's objects or regions of interest are found [33]. Dental image segmentation is beneficial in the fields of forensic dentistry, dental biometrics, and other human identifying applications in addition to the identification of dental problems [16], [34]-[37]. Dental image segmentation is beneficial in the fields of forensic dentistry, dental biometrics, and other human-identifying applications [16]. The outcomes assist dentists in the identification and diagnosis of dental disorders. Image segmentation is one of the most difficult challenges, particularly in dental X-ray images. Several segmentation techniques have been developed for efficient dental caries detection [8].

**Fully-automatic segmentation method:** The author of [19] suggested a technique for completely automated segmentation of dental diagnostic images of teeth. The key benefit is that the approach significantly improved when many images were tested. However, the drawback is that this algorithm's performance is poor when working with a large number of images.

**Edge detection method:** In the research articles [20] and [21], the author described the edge detection technique for analyzing dental X-ray images. Here, a straightforward rule-based approach was utilized to segment decaying teeth using the edge detection technique. The primary flaw in this research was the manual segmentation, which was ineffective, and the classification of caries based upon the measurement of regions. Given that dental x-ray images are often of low quality and no enhancing techniques were employed in the study.

**Contour-based segmentation method:** In the research article [38], the author described a technique for segmenting and extracting features from dental x-ray images. The images were divided into 5 groups using the k-means clustering approach to segment teeth and identify dental cavities. Gray Level Co-occurrence Matrices are used in dental diagnosis systems, like dental caries detection and person identification systems to extract features. Due to the use of bitewing x-ray images, which resulted in considerable overlapping, this experiment was unable to segment each tooth. The author has used the level-set approach for segmentation in postoperatively x-ray pictures to address the considerable overlapping problem in [39], however, this work still requires significant modifications in the segmentation process since tissues are connected with segmented teeth. To segment dental x-ray images to locate cavities, the level set active contour approach was suggested in [40]. Sobel operators were utilized for edge detection to identify the cavity. The intricacy of the timing rises as the image size does as well. Therefore, this approach is not effective for large images (64 x 64 and 256 x 256 ).

**Clustering-based segmentation method:** The pseudocoloring step of the k-means clustering algorithm was utilized to segment the plaque section and increase visibility [22]. For separating the upper and lower jaw, tooth isolation has been accomplished using a histogram-aided approach as well as spectral and spatial categorization. However, this strategy has a greater level of computational complexity.

According to the studies mentioned above, the segmentation algorithm produces a fair result, but in some cases the methods contain some inaccuracy due to user interpretation. The majority of the aforementioned segmentation algorithms are merely semi-automatic. Even though [19], and [41] attempted to segment caries, certain approaches were ineffective owing to incorrect teeth segmentation, noise, poor contrast, and atypical tooth layout. Segmentation of dental caries based on severity has not yet been done. The focus of future research may be on segmenting X-ray images using deep learning combined with optimization methods.

This research work's main contribution is:

- To create a precise, automated, U-NET-optimized dental caries segmentation model.
- A novel Explored Crow search Optimizer (CrAqOA), which is conceptually a blend of both the standard Crow Search Optimization (CSA) and Aquila Optimizer (AO), is used to fine-tune the weight function of U-NET.

The rest of this article is structured as follows: The most intriguing research in dental caries segmentation and detection is reviewed in Section II. Section III discusses the suggested model for detecting dental caries. PHASE 1: Pre-processing, PHASE 2: Three-fold Feature Extraction and PHASE 3: Segmentation using Optimized U-NET is discussed in Sections IV, V, and VI, respectively. In Section VII, the outcomes obtained using the recommended model are described. Section VIII offers a conclusion to this research article.

## 2. Literature Review

In 2022, Kumari *et al.* [1] have developed a new deep learning method for effective dental caries segmentation. As part of the pre-processing stage, noise filtering by bilateral filtering and contrast enhancement using CLAHE has been initially carried out. Additionally, the HSLnSSO, which enhances the FOC-KKC, has been utilized to segment caries and induce the optimum parameter optimization. Following the segmentation of caries, morphological procedures have been used to post-pre-process the images. The MResneXtRNN, which uses the HSLnSSO method to modify the architecture, has been used to identify caries from the segmented image. When compared to the traditional methodologies, the novel segmentation model and well-trained MResneXtRNN have demonstrated superior performance. However, this approach consumes huge processing time, and therefore it cannot be used for effective dental caries segmentation.

In 2022, Ying *et al.* [2] have developed a deep network for caries segmentation on collected tooth X-ray images. The widely utilized U-shaped network's skip connection feature was inherited by the suggested network, which also creatively applied the "vision Transformer, dilated convolution, and feature pyramid fusion methods" to improve the capacity of multi-scale and global feature extraction. Following training upon that medical self-collected and enhanced dental X-ray image dataset, the network's performance was assessed by calculating the dice similarity and pixel classification precision. The accuracy recorded by the approach is 85.6%. On the other hand, the projected model requires improvement in terms of average dice similarity (74.8%) and pixel classification precision (74.4%)

In 2022, Zhu *et al.* [3] have projected a dental caries detection model with Faster-RCNN. An open-source platform for the identification of dental caries has been developed to enable the implementation of this diagnosis method. To create the sample space and label space, the clinical samples that qualified medical professionals have acquired are first gathered and tagged. The development of a caries detection model then occurs after training and sample testing. Finally, the Flask framework has been used to distribute the model on an Alibaba cloud server once the Web platform's contents have been established and the layout has been customized using HTML and CSS programming. After the diagnosis platform has been operational for a while, patients and physicians can upload the medical images to be examined on the platform's website, where test results can be acquired. This approach is not fully automated, and the accuracy of this model is lower. In addition, the lesion location was less precise.

In 2021, Leo *et al.* [4] have designed a new HNN technique for detecting dental caries and to perform classification. A HNN is an innovative technique that is giving good results in terms of accuracy and processing time. A DNN and an ANN have been combined to create an HNN. A DNN uses a stacked sparse auto-encoder to classify images. Following this, factual evidence has been extracted from the data using "supervised fine-tuning and unsupervised pre-training". However, to categorize the layer impacted by dental caries, the ANN uses logistic regression. There are several procedures for dental input images: "Pre-processing, segmentation, feature extraction, and classification" make up the first four steps. Enamel, dentin, pulp, and root lesions have been the four main levels of caries that the HNN divides into. The suggested technique accurately classifies the caries level and produces useful results based on the supplied input image. Nevertheless, this approach is highly computational complex, and it cannot be utilized for a large database.

In 2020, Zhao *et al.* [5] have developed a TSASNet for efficient dental caries detection on dental panoramic X-ray images. To approximately localize the tooth region in the initial step, they first used an attention model that has been integrated with global and local attention modules. The attention model created in this way has automatically gathered pixel-level contextual data and detected fine tooth borders without the need for any interaction operators. They additionally segregated the real tooth area from the attention maps acquired from the first stage and used a fully convolutional network in the second stage to better gather boundary information. On the benchmark dataset of 1,500 dental panoramic X-ray images, the usefulness of TSASNet is demonstrated. The localization is not accurate, and hence this model's reliability is lower. In addition, tooth boundary and tooth roots were misclassified.

In 2018, Lee *et al.* [6] have used deep CNN for diagnosis as well as detection of dental caries on periapical radiographs. A training and validation dataset (n = 2400 [80%]) and a test dataset (n = 600 [20%]) were created from a total of 3000 periapical radiography images. For preprocessing and transfer learning, a pre-trained GoogLeNet Inception v3 CNN network was employed. For detection and diagnostic performance of the deep CNN algorithm, the ROC curve, AUC, sensitivity, specificity, positive predictive value, and negative predictive value were calculated. The diagnostic accuracies of "pre-molar, molar, and both premolar and molar models

were 89.0% (80.4–93.3), 88.0% (79.2–93.1), and 82.0% (75.5–87.1)”, respectively. Since the accuracy is lower, this approach is not effective.

In 2022, Li *et al.* [7] have developed a new multiple-scale complementary information-guided framework for dental caries detection. The statistical distribution of the plaques' color, the local-to-global structural relationship based on the HKS, and the local texture pattern based on the circle-LBP in the neighboring areas centered on the plaque area have all been parts of the crucial fused information. They developed an attention module based on CNN to even more readily focus the areas of interest in plaques, particularly for several tough situations, and to better enhance the fuzzed multiple-scale features. Rigorous testing and thorough assessments show that the approach might beat state-of-the-art techniques for a small training sample. However, this approach does not apply to a huge database. In addition, the pixel classification precision is lower.

In 2022, Imak *et al.* [8] have developed an automatic diagnosis of dental caries based on periapical images. The MI-DCNNE model was employed in the suggested technique. To boost the performance of the suggested MI-DCNNE technique, a score-based ensemble scheme was specifically used. Raw periapical images as well as an improved version of them served as the inputs for the suggested method. The Softmax layer of the suggested multi-input CNN architecture was used to do the score fusion. The effectiveness of the suggested strategy was assessed in the experimental studies using a postoperatively image dataset (340 images) that included both caries and non-caries images. It was determined from the findings that the suggested model is extremely effective in identifying dental caries. The stated accuracy rating is 99.13 percent. This approach is highly tedious, and cannot be used for timely diagnosis.

### 3. Materials and Methods

#### 3.1. Architectural Description

The global health concern of dental caries is widespread and can inevitably lead to infection of the tooth pulp and root apex. To alleviate discomfort, patients must receive a prompt as well as an efficient treatment for tooth caries. Traditional techniques of diagnosing caries infection, such as naked-eye detection and panoramic radiograph fails due to lack of accuracy. Hence, a novel deep learning architecture termed DCariesNet is suggested in this research work, to differentiate between the two caries grades using X-ray images.

The newly projected DCariesNet encapsulates three major phases:” (a) Phase1: Pre-processing, (b) Phase 2: Feature Extraction, and (c) Phase 3: Dental Caries Segmentation. The architecture of DCariesNet is shown in Fig.1. The mechanism undergone in each of these stages is furnished below:

The dental X-rays of the patients are observed, and they are represented using the symbol  $D_i^{inp}; i = 1, 2, \dots, N$  (for simplicity). Here,  $N$  points to the count of X-ray inputs.

(a)Phase1: Pre-processing- This is the initial phase, and here the collected X-ray images  $D_i^{inp}$  are pre-processed via (a) Noise Removal using Partition Supported Median, Interpolation, and Discrete Wavelet Transform (NRPMID), (b) morphological operations (dilation, erosion, opening, and closing) and (c) histogram equalization. The pre-processed image acquired after noise removal and contrast enhancement is denoted using the symbol  $D_i^{pre}$ .

(b) Phase 2: Feature Extraction-The three-fold features, like  $LBP(f^{LBP})$ ,  $LDP(f^{LDP})$ , and  $LOOP(f^{LOOP})$  are extracted from  $D_i^{pre}$ . These features are amalgamated, and they are denoted using the symbol  $G = f^{LBP} + f^{LDP} + f^{LOOP}$ . Using  $G$  (fused features), the dental caries detection phase is trained.

(c) Phase 3: Segmentation Phase- The segmentation of the dental X-ray images is complicated, owing to the variation in the shape as well as intensity (within the same X-ray dental images and from one image to another). Therefore, this phase is modeled using an optimized U-NET-based CNN framework. The weight function of U-NET is optimized using a new Aquila Explored Crow search Optimizer (CrAqOA). This CrAqOA model is devised by blending the concepts of the standard AO and CSA, respectively. This optimized U-NET-based CNN framework is trained with  $G$ . The outcome from optimized U-NET is the segmented outcome (i.e. caries affected area). This approach will support the dentist in the early detection of dental caries.

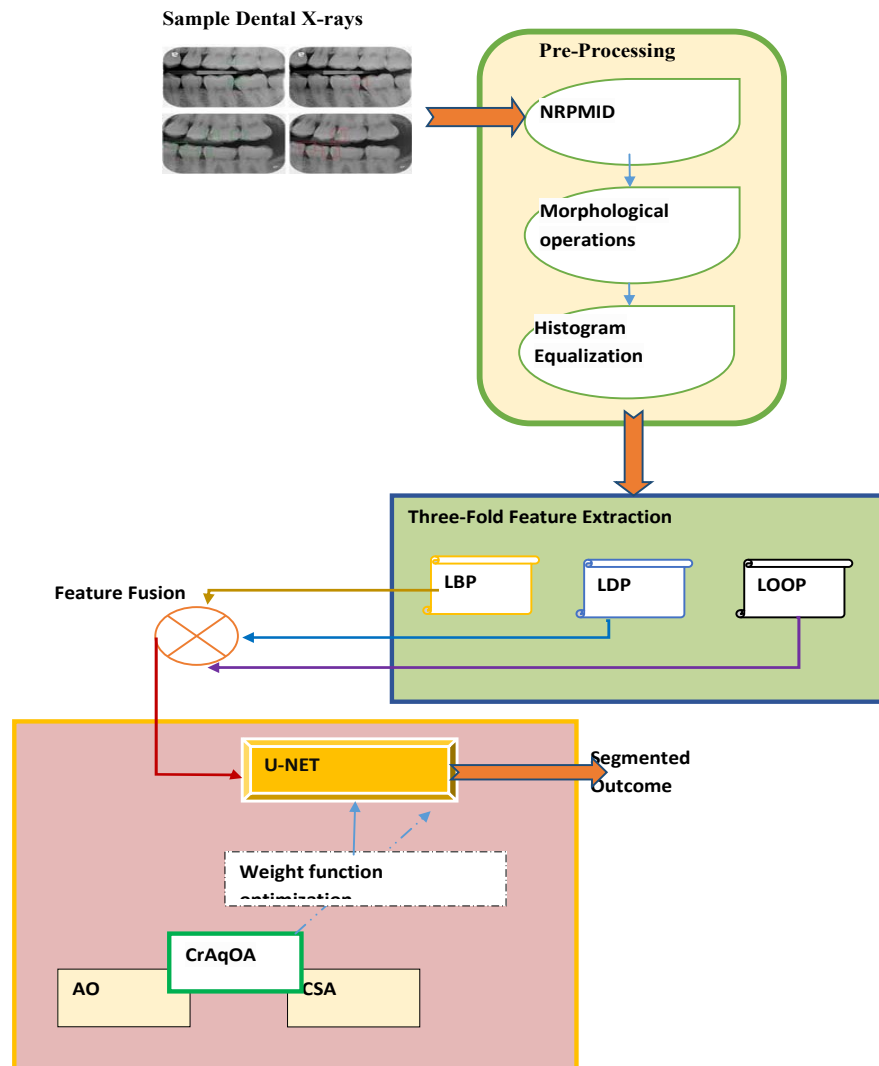


Figure 3.1 . DcariesNet: Architectural Representation

### 3.1.1. Phase 1: Pre-Processing

The input X-ray images  $D_i^{imp}$  are pre-processed via (a) “Noise Removal using Partition Supported Median, Interpolation, and Discrete Wavelet Transform (NRPMID)”, (b) morphological operations (dilation, erosion, opening, and closing), and (c) histogram equalization. The pre-processing phase is diagrammatically shown in Fig.2.

SS

### Figure 3.2. Pre-processing Phase

#### 3.1.1.1. NRPMID

The image  $D_i^{imp}$  is first pre-processed using the NRPMID method. D spans 512 \* 512 pixels. This methodology uses eight concepts, including "Mean filter, Median filter, Bi-linear interpolation-based filter, Partition based Median filter, Bi-cubic interpolation-based filter, Partition based Bi-cubic interpolation-based filter, Partition based Lanczos interpolation-based filter, and Partition based HAAR wavelet transform based filter", to eliminate impulse noise or salt and pepper noise from Dental X-RAY images. This process utilizes cutting and multiple-size window concepts as well as multi-size window and trimming concepts. The

NRPMID technique produces a noise-free result, and it is denoted by the symbol  $D_i^{NRPMID}$ . Then, the morphological openings are applied to the noise-free images  $D_i^{NRPMID}$ .

### 3.1.1.2. Morphological Operation

Digital images are processed depending on their forms using a variety of image processing techniques known as morphological operations [47]. Each image pixel in a morphological procedure corresponds to the number of other pixels in the region.  $D_i^{NRPMID}$  is subjected to morphological processes, such as dilatation, erosion, opening, and closure. The morphological operations are shown in Fig.3.

**Erosion:** The image pixels are reduced in size by erosion, or pixels on object boundaries are removed by erosion. The erosion procedure is first carried out by traversing the structuring element across the image object. The following equation (Eq.(1) and Eq. (2)) is used to determine the output pixel values.

$$\text{Pixel (output)} = 1 \text{ \{if FIT\}} \quad (1)$$

$$\text{Pixel (output)} = 0 \text{ \{otherwise\}} \quad (2)$$

FIT refers to the condition in which all of the pixels in the structuring element completely encircle the pixels of the object.

**Dilation:** Dilation enlarges the pixels in the image or extends pixels to the edges of objects. The dilation operation is first executed by iterating over the structuring element over the image object. Using Eq. (3) and Eq. (4), the output pixel values are determined.

$$\text{Pixel (output)} = 1 \text{ \{if HIT\}} \quad (3)$$

$$\text{Pixel (output)} = 0 \text{ \{otherwise\}} \quad (4)$$

An object is said to have been HIT whenever at least one of the pixels in the structuring element covers the pixels of the object.

The two most often employed compound procedures are: (a) Closing (by first conducting dilatation and then erosion), and (b) Opening (by first performing erosion and then dilatation). The opening is typically employed to reconstruct or retrieve the noise-free image to the greatest degree feasible. The purpose of the closing is often to restore the narrow gaps and lengthy, thin gulfs and to smooth out the contour of the deformed image. Closing is further employed to eliminate the tiny gaps in the noise-free image. The resultant acquired after performing the morphological operations is represented using the symbol  $D_i^{Morp}$ . Onto  $D_i^{Morp}$ , the histogram equalization is performed to enhance the quality of the image.

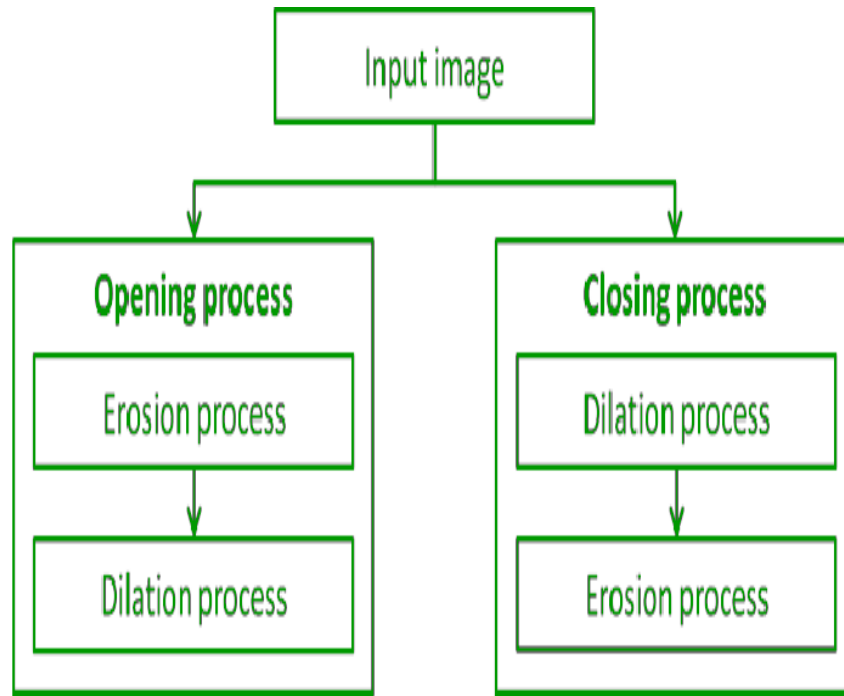


Figure 3. Morphological Operations

### 3.1.1.3. Histogram Equalization

The input to histogram equalization is  $D_i^{Morp}$ . A computer image processing method called Histogram Equalization Park *et al.* [32] is being used to enhance contrast in images. This is achieved by successfully extending the intensity range of the image and dispersing out the most common levels of intensity. Whenever the useful information is represented by near contrast values, this strategy often boosts the overall contrast of the images. It makes it possible for regions with less local contrast to acquiring significant contrast. The outcome acquired from histogram equalization is a contrast-enhanced noise-free image, and it is denoted as  $D_i^{pre}$  (pre-processed image). From  $D_i^{pre}$ , the three-fold features are extracted.

### 3.1.2. Phase 2: Three-Fold Feature Extraction

The three-fold features, like LBP, LDTP, and LOOP are extracted from the pre-processed image  $D_i^{pre}$ . The three-fold extracted features are diagrammatically shown in Fig.4.

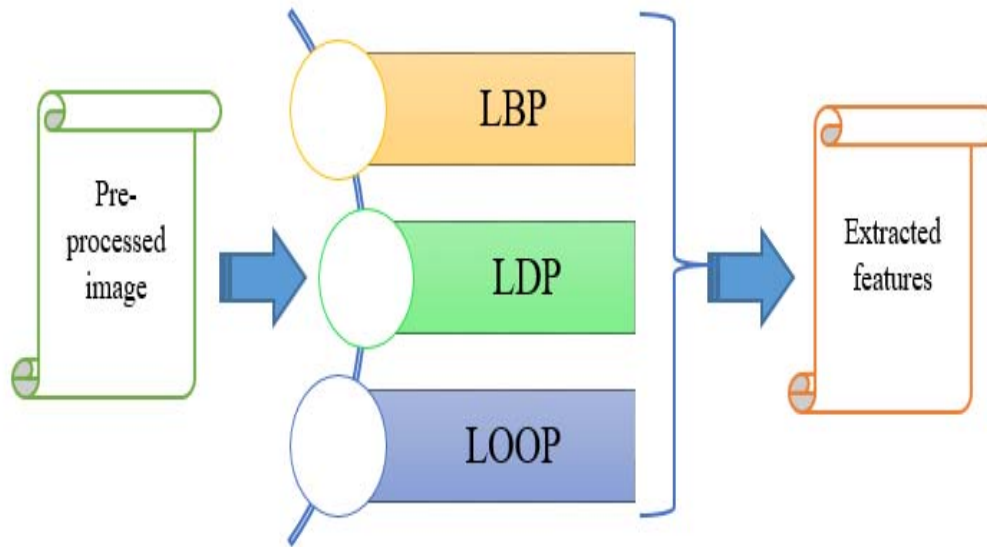


Figure 4. Three-fold feature extraction

### 3.1.2.1. LBP

The LBP is considered one of the most effective texture descriptors. It was introduced by Mamoun *et al.* [17], for the first time, and it is used to represent the local features of an image which means the key points of an image. The classic LBP operator is described as a window of  $3 \times 3$  pixels. The centre pixel of this window is considered a threshold; if the neighbouring pixel's value is less than the threshold value, the pixel value is labelled 0, else it is 1. This method will generate an 8-bit binary number converted to a decimal number, as shown in Fig. 2.

One of the best texture descriptors is known as LBP [18]. It is employed to illustrate an image's regional characteristics, or its focal points. A window of  $3 \times 3$  pixels is used to define the traditional LBP operator. Mathematically, the LBP descriptor can be expressed as per Eq. (5) to Eq. (8), respectively.

$$f_{A,B}^{LBP}(pix_c) = \sum_{b=0}^{B-1} Q(pix_b - pix_c) \cdot 2^b \quad (5)$$

$$Q(M) = \begin{cases} 0 & M < 0 \\ 1 & otherwise \end{cases} \quad (6)$$

Here,  $pix_c = pix(M, O)$  is the central pixel of  $D_i^{pre}$  at location  $(M, O)$ . In addition,  $pix_b = pix(M_b, O_b)$  is the central pixel's neighborhood.

$$M_b = M + D \cdot \cos\left(2\pi \frac{b}{B}\right) \quad (7)$$

$$O_b = O - D \cdot \sin\left(2\pi \frac{b}{B}\right) \quad (8)$$

Here,  $B$  points to the count of neighboring pixels and  $D$  is the distance from the central pixel  $pix_c$  in  $D_i^{pre}$ . The extracted LBP based features is represented as  $f^{LBP}$ . An illustration of code generation with LBP is shown in Fig.5.



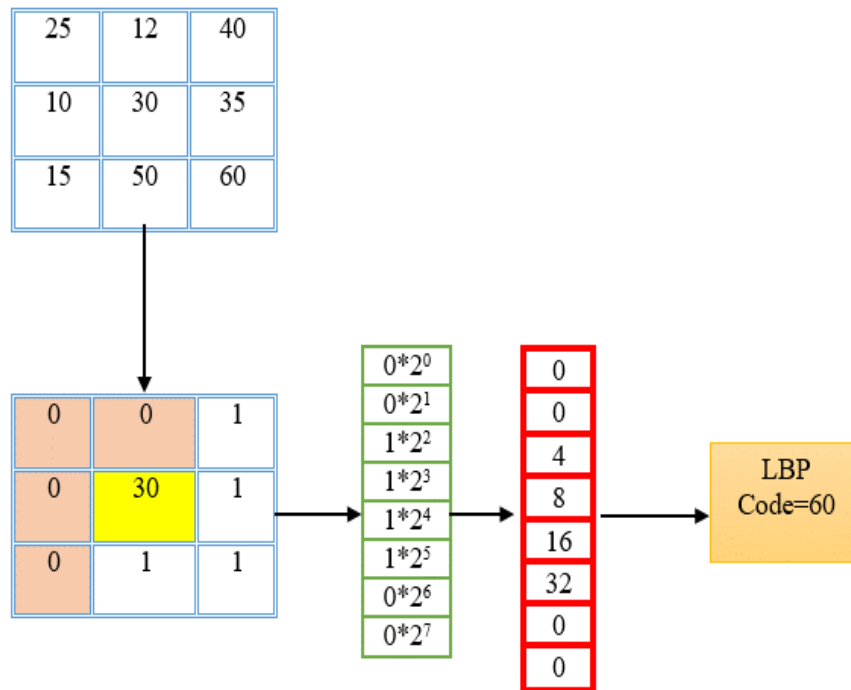


Fig.5 LBP code generation: An Illustration

### 3.1.2.2. LDP

The primary axis in each neighborhood is how the LDP operator, a potent texture operator retrieves the texture data. The LDP [49] operator just contains the essential data, unlike other operators that attempt to take into account all available data, which occasionally may cause code problems. It performs well and is used for detecting dental cavities. At  $(p_k, p_l)$  of  $D_i^{pre}$ , the intensity is denoted as  $I_u$ . In the 3\*3 neighborhood of  $(p_k, p_l)$ , the intensity of a pixel is pointed as  $I_s; s = 0, 1, 2, \dots, 7$ . The eight responses of the Kirsch masks, with intensity,  $I_s$  are denoted as  $k_s; s = 0, 1, 2, \dots, 7$ . The  $c^{th}$  highest Kirsch activation is denoted as  $k_c$ . The neighboring pixels with Kirsch response higher than  $k_c$  is assigned as 0, and the others are labeled as 0. Mathematically, LDP can be given as per Eq. (9) and Eq. (10), respectively. The pixel information is shown in Fig. 6.

$$f_c^{LDP}(p_k, p_l) = \sum_{s=0}^7 v(k_s - k_c) \cdot 2^s \quad (9)$$

$$v(p) = \begin{cases} 0 & v \geq 0 \\ 1 & \text{otherwise} \end{cases} \quad (10)$$

where  $f^{LDP}$  are the extracted LDP-based features.



Fig.6 Pixel Information: center pixel and neighboring pixels

### 3.1.2.3. LOOP

LOOP [42] present a nonlinear amalgamation of LBP and LDP. At pixel  $(u_c, v_c)$ , LOOP can be given as per Eq. (11) and Eq. (12), respectively. The notation  $Int_{cen}$  denotes the intensity of  $D_i^{pre}$  at  $(u_{cen}, v_{cen})$ . In the 3\*3 matrix, the intensity of the pixels (excluding the center pixel) is pointed as  $Int_m$ . Each of the pixels is assigned a value  $\omega_m$  (a value between 0 and 7).

$$f^{LOOP}(u_{cen}, v_{cen}) = \sum_{m=0}^7 h(Int_m - Int_{cen}). 2^{\omega_m} \quad (11)$$

$$h(u) = \begin{cases} 0 & \text{if } u \geq 0 \\ 1 & \text{otherwise} \end{cases} \quad (12)$$

Where,  $f^{LOOP}$  are the extracted LDP-based features.

All these extracted features are amalgamated together as  $G = f^{LBP} + f^{LDP} + f^{LOOP}$ . Using  $G$ , the caries detector (segmentation phase) is trained. The feature fusion phase is exhibited in Fig.7.

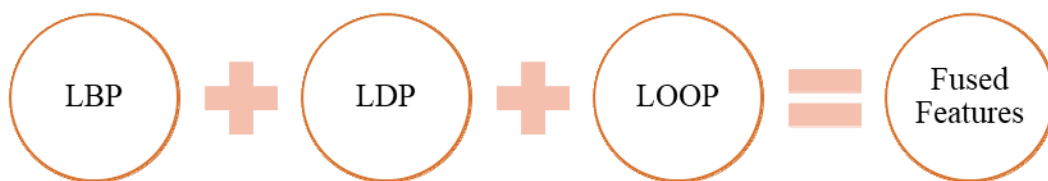


Fig.7 Feature Fusion

### 3.1.3. Phase 3: Segmentation with optimized U-NET

This phase is modeled using an optimized U-NET-based CNN framework. The weight function of U-NET is optimized using a new CrAqOA. This CrAqOA model is devised by blending the concepts of the standard AO and CSA, respectively. This optimized U-NET-based CNN framework is trained with  $G$ .

### 3.1.3.1. Optimized U-NET

The U-Net network [43], an evolution of the fully convolutional network (FCN), has become the foundation of medicinal image segmentation since the semantic segmentation impact of FCN is relatively harsh [21]. Olaf Ronneberger introduced the semantic segmentation network known as U-Net in 2015. To compensate for the data lost during the classification step, several feature maps are added to the upsampling in the down-sampling stage. Fig. 8 depicts the structure of U-NET. There are expansion and contraction paths in U-Net. A contraction pathway, or downsampling, can be observed on the left side of Fig.8. It consists of two 3\*3 convolutional layers and a 2\*2 maximum pooling layer with a stride of 2. Rectified linear unit (ReLU) is the activation function. Typically, the fully connected layer has been omitted from the standard image categorization network. On  $G$ , it does a convolution kernel pooling operation to gather contextual semantic information to address the classification issue in image segmentation. Upsampling, an extension route that could also locate segmentation tasks, is shown on the right. There is a symmetry between up- and downsampling. Two 3\*3 convolutions are then employed after connecting a 2\*2 convolutional layer to lessen the number of feature channels. Finally, a 1\*1 convolutional layer with an unpadding structure is added to map the necessary amount of feature vectors.

During upsampling, the U-Net network undergoes a significant structural shift that allows it to create more distinctive channels. In addition, feature fusion is carried out distinctly by U-Net and FCN. While U-Net splices the feature maps to create more channels, FCN inserts the feature maps piece by piece. When doing image segmentation, the learning algorithm (proposed hybrid optimization-CrAqOA) uses fewer sets of data, can converge on a limited quantity of data, and produces results rapidly.

Processing medical images offer unique benefits when using U-Net. Elastic deformation has been employed to finish the data augmentation process to address the issue of the lack of sample images in medical imaging. Since elastic deformation occurs mostly in living cells, it's a sort of deformation that is ideal for use in medical image processing. To provide the neural network model with strong elastic deformation adaptability whenever the time series is insufficient, the method of data enhancement is used to educate it on the interpretability of elastic deformation. If confronted with a medical image that has been elastically bent, it can appropriately finish the segmentation.

An attention module is added to the U-Net to increase segmentation speed. Human visual attention systems can be divided into two categories: "bottom-up data-driven attention mechanisms and top-down target attention mechanisms". Both techniques are capable of learning the task-specific components from a sizable quantity of information. A bottom-up, data-driven attention mechanism is employed by the suggested network. The correlation between feature channels serves as the starting point for the attention module, which also takes into account their interdependencies. Those elements that have a minor influence on the present segmentation are efficiently suppressed by the network's self-learning process, while the weight of advantageous features is increased. Fig.9 illustrates its modular architecture.

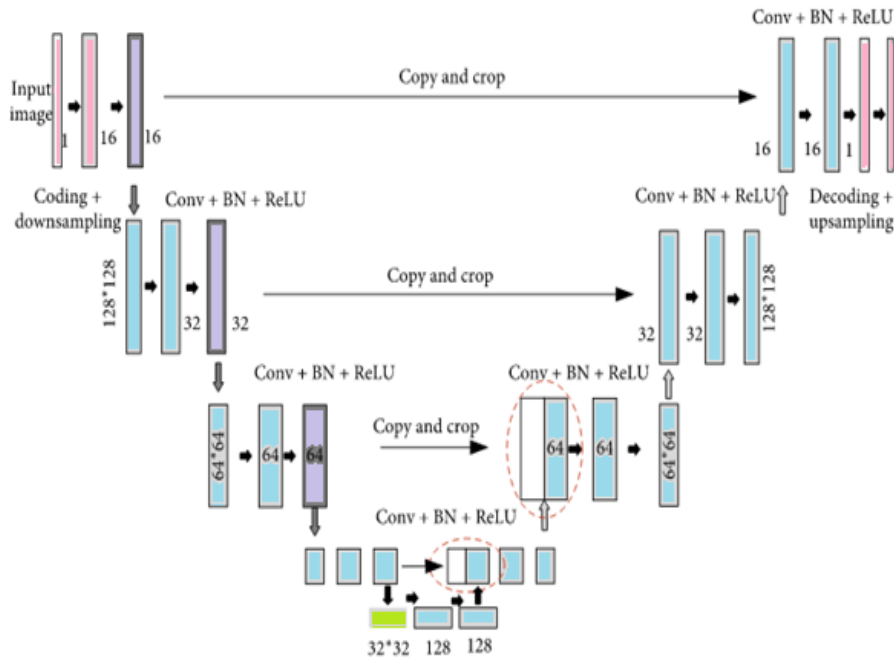


Fig 8.U-NET Architecture

Weighted cross-entropy, which is computed using Eq.(13) and Eq. (14), is used in the energy function (*loss*) of network training.

$$loss = \sum_{j \in \mathcal{Y}} \beta(j) \cdot \log(p_{\varpi}(j)) \quad (13)$$

$$p_{\varpi}(j) = \frac{\exp(\delta_{\varpi}(j))}{\sum_{\varpi'} \exp(\delta_{\varpi'}(j))} \quad (14)$$

where  $\delta_{\varpi}(j)$  is the activation function for the  $j$ -th pixel's  $\varpi$ -th feature channel. The number of classifications (presence/absence of dental caries, totally 2) is  $Y$ . The maximal functionality is about  $p_{\varpi}(j) \cdot \beta(j)$  is the weight of a pixel in the training composition; the higher the weight, the more significant the pixel is.

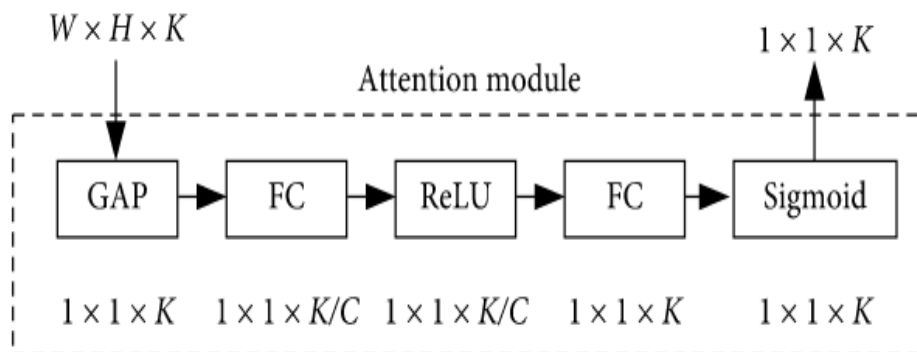


Fig 9.Attention Module's Structure

To improve the segmentation accuracy, this loss function ( $loss$ ) needs to be decreased. So, the weight function  $W$  of U-NET is optimized with a novel hybrid optimization model. The reduction of the loss function ( $loss$ ) is the research's prime objective. This is mathematically given in Eq. (15).

$$obj = \min(loss) \quad (15)$$

The attention module conducts two FC layer conversions after performing GAP on each channel's feature map to produce a vector of  $1*1*k$ . Between two FC layer conversions, dimensionality reduction and augmentation are carried out, and Sigmoid and ReLU activation functions are applied. A GAP enhancement approach called SAP is suggested to address the single-category problem in GAP and better understand the geographical distribution of the image. The SAP process is shown in Fig.10. The outcome from the network is a segmented outcome that portrays the information regarding the affected regions.

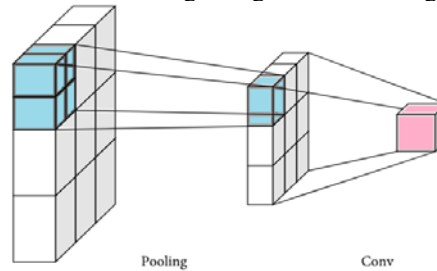


Fig 10 SAP process

**Aquila Explored Crow search Optimizer (CrAqOA):** The CrAqOA model is developed by conceptually amalgamating the AO and CSA models, respectively. AO [44] and CSA [45] are highly convergent. Interestingly, while blending AO and CSA, the convergence of the solutions boosted up, and hence assists in enhancing the segmentation accuracy. The AO model mimics Aquila's hunting behavior. The CSA model has been developed with the intelligent behavior of the crows in hunting its food. In CrAqOA, the AO model has been induced within CSA. The input to CrAqOA is the weight function of U-NET. The steps followed in the AECSO model are manifested below:

**Step 1- Parameter Initialization:** The population ( $P$ ) of  $N$  – the count of search agents (crows and Aquila's) is initialized. The current iteration is denoted as  $itr$ , and the maximal iteration is pointed as  $\max^{itr}$ . The awareness probability ( $A$ ), as well as flight steps size, ( $B$ ) is also initialized.

**Step 2- Search Agent Initialization-** The memory matrix as well as individual crows is initialized. In the  $t$  – dimension search space,  $N$  – the count of search agents is initialized. The solution passed as input to CrAqOA models is the weight function  $W$  of U-NET, and it is delineated as the position of the search agent. The position of every search agent is denoted as  $Z^i = \{Z^{i,1}, Z^{i,2}, Z^{i,3} \dots Z^{i,d}\}$ . Since there isn't any experience in the initial position, the initial memory matrix is assumed to be the same as the initial position.

**Step 3- Fitness Evaluation:** The fitness of every search agent in the search space is evaluated, using Eq. (15).

**Step 4- Proposed Solution Update phase:** In the  $t$  – dimension search space, the new location is generated for every search agent. To find the place where the crow  $i$  has hidden its food, the crow  $j$  follows crow  $i$ . The position update of the crow  $i$  can be updated via two conditions:

Case1:  $i^{th}$  position of the crow is not found by the crow  $j$ . In this case, the following steps are undertaken:

1. A random number  $R[0,1]$  is generated.
2. If  $R[0,1] \leq 0.5$ , the position of the solutions is updated using the improved expanded exploration stage of Aquila. Therefore, global solutions can be acquired without getting trapped in the local optima. Moreover, the solutions do not go beyond the search space. Since the search agent ( $j$ ) is unable to find the position  $i$ , the crow  $j$  tries to explore from high sores to determine the search space  $i$ . This behavior is mathematically modeled as per Eq. (16).

$$Z^{i,(itr+1)} = Z^{best(i,itr)} * m^{itr} * \left(1 - \frac{itr}{\max^{itr}}\right) + \left(Z^{mean(i,itr)} - Z^{best(i,itr)}\right) * rand * Z^{worst(i,itr)} \quad (16)$$

Here,  $Z^{i,(itr+1)}$  is the next position of the crow  $j$  during its searching behavior. In addition,  $Z^{best(i,itr)}$  and  $Z^{worst(i,itr)}$  is the best as well as the worst position of the search agent, respectively. Moreover,  $Z^{mean(i,itr)}$  is the mean value of the location corresponding to the current position. In addition,  $m^{itr}$  is the memory of the search agent  $i$ , during its searching behavior. Since the memory function and position of the worst search agent are newly added, the convergence gets increased.

3. If  $R[0,1] > 0.5$ , then the position of solutions is updated using the improved narrowed exploration stage of Aquila. Since  $j$  is unable to find the position  $i$ , it randomly circles the areas that  $i$  have travelled. This form of searching is termed as contour flight with a short glide attack. This is mathematically given in Eq. (17).

$$Z^{i,(itr+1)} = \frac{Z^{best(i,itr)} * Levy(\chi) + Z^{R(i,itr)} + (y-x) * rand}{m^{(i,itr)} * Z^{worst(i,itr)}} \quad (17)$$

Here,  $Levy(\chi)$  is the levy flight distribution, and  $Z^{R(itr)}$  is the random solution within  $[1, N]$ , and  $rand$  is a random number.

Case 2: Crow  $j$  finds the position of the crow  $i$ . The position update is based on awareness probability ( $A$ ). The proposed solution updating procedure is manifested below:

1. A random number  $r$  is initialized between 0 and 1.
2. If  $(r \geq A)$ , the position of the search agent is updated as per Eq. (18).

$$Z^{i,(itr+1)} = Z^{i(itr)} + r^i * B * (m^{i(itr)} - Z^{i(itr)}) \quad (18)$$

Here,  $r^i$  is the random number  $[0,1]$ .

3. If  $(r < A)$ , the position of the search agent is updated using a new mathematical expression shown in Eq. (19; instead of random updating in CSA).

$$Z^{i,(itr+1)} = Z^{gbest(i,itr)} + Z^{i(itr)} * C(0,1) \quad (19)$$

The global best position  $Z^{gbest(i,itr)}$  as well as  $C(0,1)$  are newly added to enhance the convergence of the solutions. But, the global search behavior is also boosted with  $Z^{gbest(i,itr)}$ . Moreover,  $C(0,1)$  prevents the solutions from easily falling into the local optimum.

**Step 5:** Verifying that each crow's new position is practical. Change the crow's posture at all feasible positions. If not, it is not updated.

**Step 6:** Determine the fitness value for each crow's new position.

**Step 7:** Involve updating each crow's memory matrix.

**Step 8:** Repetition of Steps 4 through 7 until the terminating criterion is met.

The outcome acquired from the optimized U-NET is the segmented one (i.e. isolates the affected region from the non-affected ones).

## 4. Result and Discussion

### 4.1. Experimental Setup

The anticipated DcariesNet has been put into practice using MATLAB. Data from the following source was used to evaluate the project: <https://www.kaggle.com/datasets/daverattan/dental-xrarty-tfrecords> (Date: 2023-01-08). 50% of the data obtained were used to train the model, while the remaining 50% were utilized to test the predicted model. The sample images and their corresponding outcomes are manifested in Fig.11. Accuracy, specificity, precision, sensitivity, F1-score, and MSE have all been included in the evaluation. The projected model has been evaluated in comparison to other current models, including otsu thresholding, UNET, CSA-based UNET, and AO-based UNET.

### 4.2. Training Percentage validation: Proposed Vs Existing Models

The anticipated model's performance is compared to the current models of Otsu thresholding, UNET, CSA-based UNET (also known as CSO-based UNET), and AO-based UNET (also known as AqOA-based UNET). Accuracy, specificity, sensitivity, F1-score, and MSE have all been included in the evaluation. The training percentage (TP) was varied for each evaluation, starting at 50, 60, 70, 80, and 90, respectively. Fig.12 displays the outcomes that were documented. When compared to the current models, the projected model has produced the most noteworthy results, according to the results obtained. At TP=90, the projected model's segmentation

accuracy is 95.8%, which is the highest reported. The suggested approach outperforms current methods like Otsu thresholding, UNET, CSA-based UNET, and AO-based UNET in terms of accuracy at TP=90 by 20.53%, 9.803%, 6.01%, and 5.98%, respectively. Additionally, at TP=90, the predicted model's accuracy was 9.5%, which is better than UNET alone. Thus, it is evident that the anticipated model's accuracy level using UNET alone would only be up to 85%, which is insufficient for dental caries segmentation. Additionally, at TP=70, CSA and AO alone obtained accuracy levels of 88.2% and 87.9%, respectively, which are both lower than the accuracy level of the proposed model (93.4%). It is blatantly obvious that the projected model's ability to achieve the best segmentation accuracy was only possible thanks to precisely adjusting the weight of U-NET using a novel hybrid optimization model. Additionally, the main goal of this study endeavor is to minimize loss (also known as an error). The MSE validation has been done as a result to show how much better the predicted model is. When comparing the projected model to the current models, analysis of the obtained results revealed that it had the lowest MSE. This resolves the misclassification problem that existed with the current models [8], [7], [14], [19], [41], and [46]. At TP=90, the projected model has recorded the least MSE as 5.107, which is superior to Otsu thresholding=24.59, UNET=14.409, CSA-based UNET=10.8, AO-based UNET=10.78. Thus, the projected model is said to be highly applicable for dental caries segmentation. In addition, the projected model recorded the highest F1 measure. The F1-measure recorded by the projected model at TP=90 is 92.6%, which is 19.87%, 13.59%, 9.01%, and 9.28% better than Otsu thresholding, UNET, CSA-based UNET, AO-based UNET, respectively. In addition, the projected model has recorded the highest precision at 92.7%, which is indeed the best score. Moreover, the precision of the projected model at TP=80 is 92.2%, which is 25.01%, 19.78%, 12.83%, and 11.93% better than Otsu thresholding, UNET, CSA-based UNET, AO-based UNET, respectively. In addition, the projected model has recorded the highest sensitivity as 87.9% at TP=50, 88.9% at TP=60, 91.09% at TP=70, 92.6% at TP=80 and 94.29% at TP=90. The lower sensitivity issue has been recorded in most of the existing models [5], and [12]. However, this research effectively extracted three-fold traits to resolve the issue. Additionally, the projected model has the maximum specificity for each TP variant. The anticipated model's specificity at TP=90 is 93.18%, which is indeed the greatest mark. The anticipated model is considered to be highly appropriate for segmenting dental caries as a whole.

#### 4.3. K-Fold Validation: Proposed Vs Existing Models

To successfully verify the performance of the projected model, the K-fold validation is used. By changing the K-values from 2, 3, 5, 6, and 8, correspondingly, the assessment has been made. Accuracy, specificity, sensitivity, precision, F1-score, and MSE have all been included in the evaluation. In Fig. 13, the results obtained are represented visually. The maximum accuracy value was 93.6% for the predicted model, outperforming Otsu thresholding by 20.59% and UNET by 5.71%. Additionally, the accuracy level of 72.9% with Otsu thresholding can only be detected at K=6. But, while using UNET, the segmentation accuracy of 83.3% can only be recorded at K=6. On the other hand, with the optimized UNET, the accuracy level got boosted and reached the maximal value of 92.2% at K=6. The projected model has also recorded the highest F1 measure, specificity, sensitivity as well as precision. The highest F1 measure of 94.5% has been recorded by the projected model at K=6. The precision recorded by the projected model at K=2 is 85.7%, K=3 is 88.8%, K=5 is 89.7%, K=6 is 90.16% and K=8 is 90.79%. The projected model has recorded the highest sensitivity as 93.2% at K=6, which is 15.8%, 7.66%, 3.41%, and 3.74% better than existing models like Otsu thresholding, UNET, CSA-based UNET, AO-based UNET, respectively. The projected model has recorded the maximal specificity as 95.5% at K=6. The least MSE value for each adjustment in the K-value also is noted by the projected model. At K=6, the predicted model's MSE outperforms current methods like Otsu thresholding, UNET, CSA-based UNET, and AO-based UNET by 75.15%, 59.14%, and 44%, and 45.6%, respectively. The predicted model's performance has improved owing to the noise-free images and sophisticated pre-processing approaches. Therefore, it is claimed that the projected model is very relevant for precise dental caries segmentation.

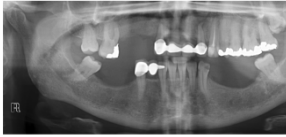
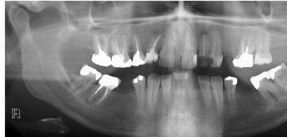

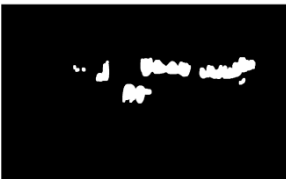








#### 4.4. Analysis of the performance of suggested model: Varying epoch

The projected model is assessed by varying the epochs from 20, 40, 60, 80, and 100, respectively. On analyzing the acquired outcomes (shown in Fig. 14), the projected model has recorded the highest value for every variation in the epochs. At 100<sup>th</sup> epoch, the utmost accuracy of 95.47% has been recorded by the projected model, and this value is 2.39%, 2.05%, 1.61%, and 1.06% better than the accuracy recorded by the existing models at 20<sup>th</sup> epoch, 40<sup>th</sup> epoch, 60<sup>th</sup> epoch, 80<sup>th</sup> epoch, and 100<sup>th</sup> epoch, respectively. In addition, the maximal F1-measure of 97.2% has been recorded by the suggested approach at 100<sup>th</sup> epoch, and this value is the most optimal one. The highest precision has been recorded by the projected model for every variation in the epoch scores. At TP=90, the precision of the projected model at 100<sup>th</sup> epoch is 98.13%, which is better than 17.42% at 20<sup>th</sup> epoch, 12.41% at 40<sup>th</sup> epoch, 4.47% at 60<sup>th</sup> epoch, and 3.82% at 80<sup>th</sup> epoch. The sensitivity recorded by the projected model at 100<sup>th</sup> epoch corresponding to 90<sup>th</sup> TP is 97.5%, which is better than the sensitivity recorded by the







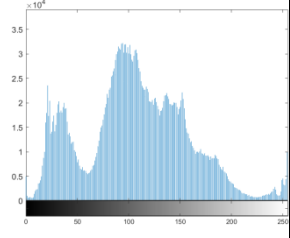
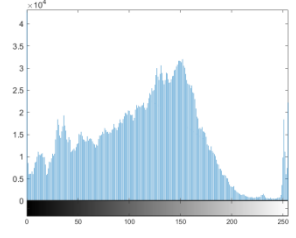
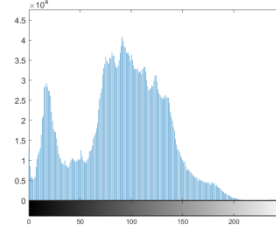
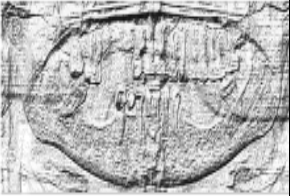






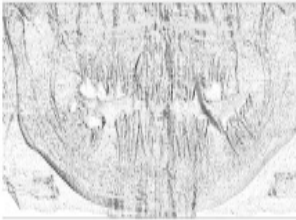
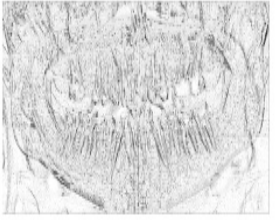
projected model at 20<sup>th</sup> epoch=94.6%, 40<sup>th</sup> epoch=96.27%, 60<sup>th</sup> epoch=96.7%, 80<sup>th</sup> epoch=97.13%. In addition, the projected mode has also recorded the least MSE for every variation in the epochs. As a whole, the projected model is applicable for the accurate and timely detection of dental cavities.

**4.5. Analysis of K-Fold of the suggested model: Varying epoch**

The projected model has been validated by varying the k-values for every variation in the epochs. The evaluation has been made in terms of “accuracy, specificity, precision, sensitivity, F1-score and MSE, respectively. All the assessments have been made by varying the K-Fold (K) from 2, 4, 5, 6, and 8, respectively. On analyzing the outcomes (shown in Fig.15), the projected model has recorded the most optimal performance for every variation in the k-values. The optimal tuning of the U-NET with CrAqOA is the major reason behind this improvement. For 100<sup>th</sup> epoch, the accuracy recorded by the projected model at K=8 is 94.02%, which is better than 91.6% recorded at K=2, 91.7% recorded at K=4, 92.4% recorded at K=5, 93.06% recorded at K=6. In addition, the projected model has recorded the maximal F1-measure, specificity, sensitivity as well as precision for every variation in the epochs. In addition, the MSE of the projected model at 100<sup>th</sup> epoch corresponding to K=8 is 5.9%, which is perhaps the least value compared to existing models (at the same epoch level). Thus, the projected model is suggested to be a suitable approach for dental cavities segmentation.

DDDD	Sample 1	Sample 2	Sample 3
Sample Images			
Dilation			
Erosion			
Opening			



<p><b>Closing</b></p>			
<p><b>NRPMI D</b></p>			
<p><b>Histogram equaliza tion</b></p>			
<p><b>LBP</b></p>			
<p><b>LDP</b></p>			
<p><b>LOOP</b></p>			

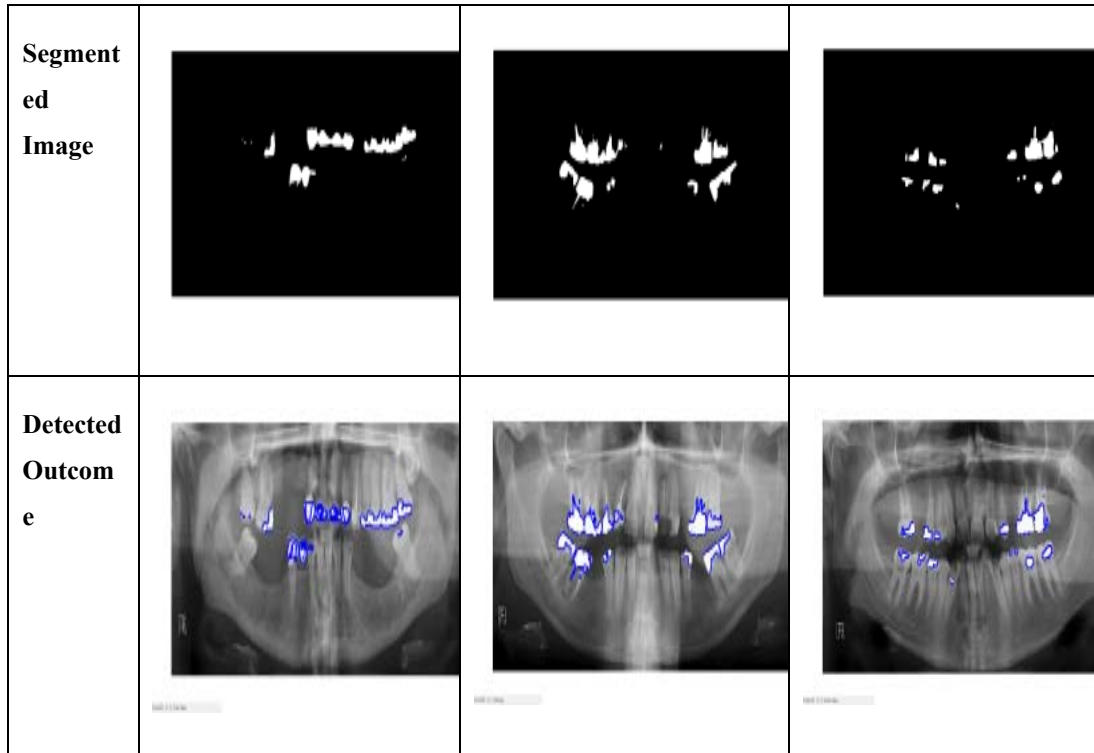
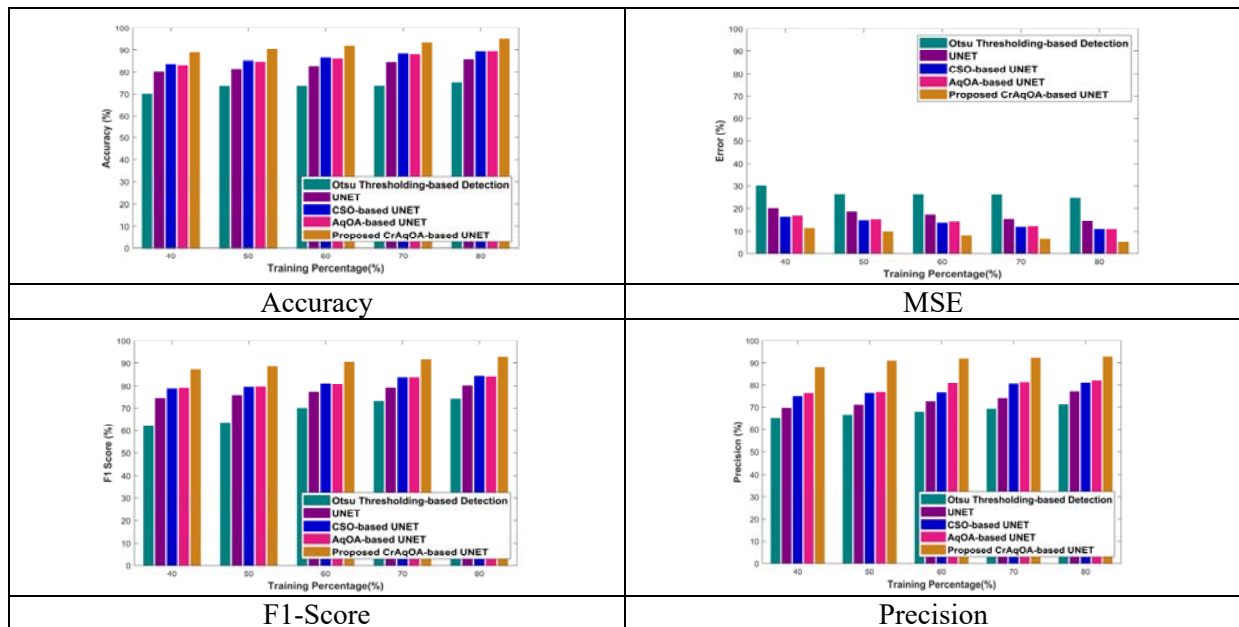


Figure 11. Sample Images and their corresponding outcomes



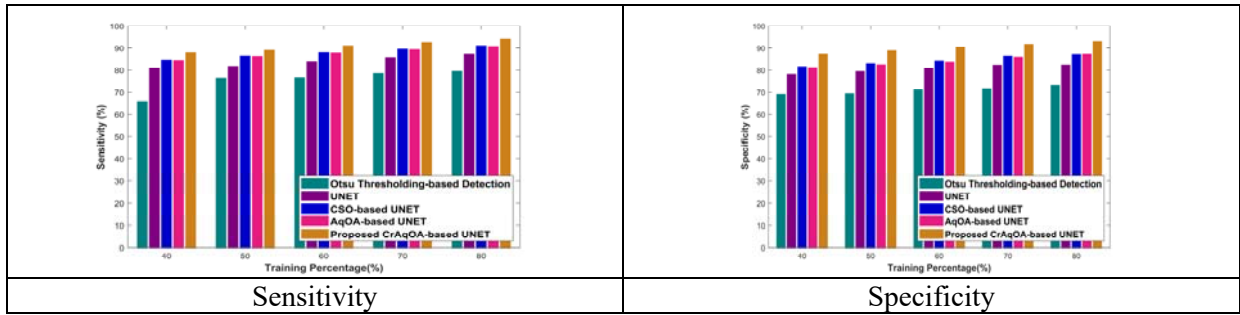


Figure 12. Comparative Analysis of the projected model and existing models by varying Training Percentage

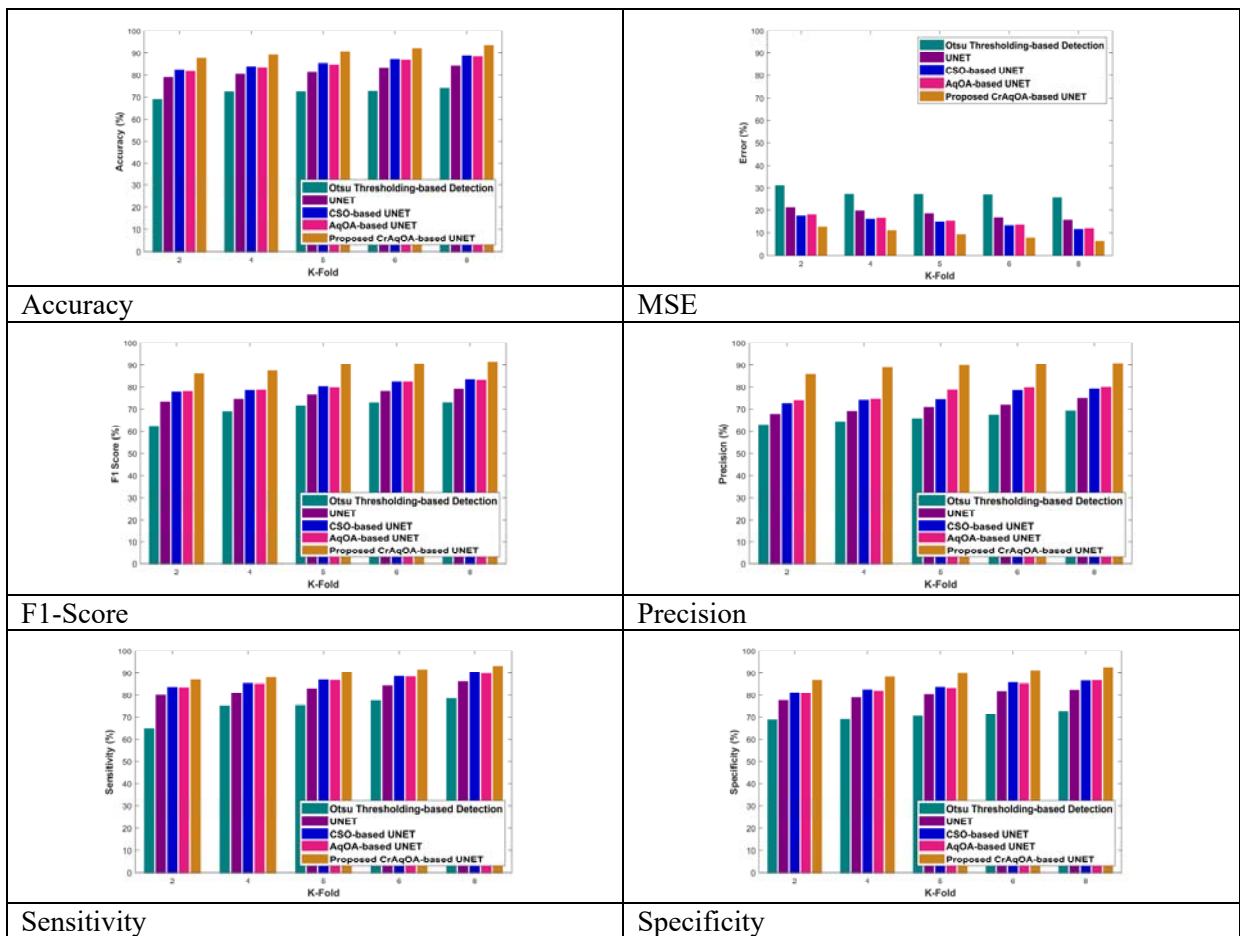
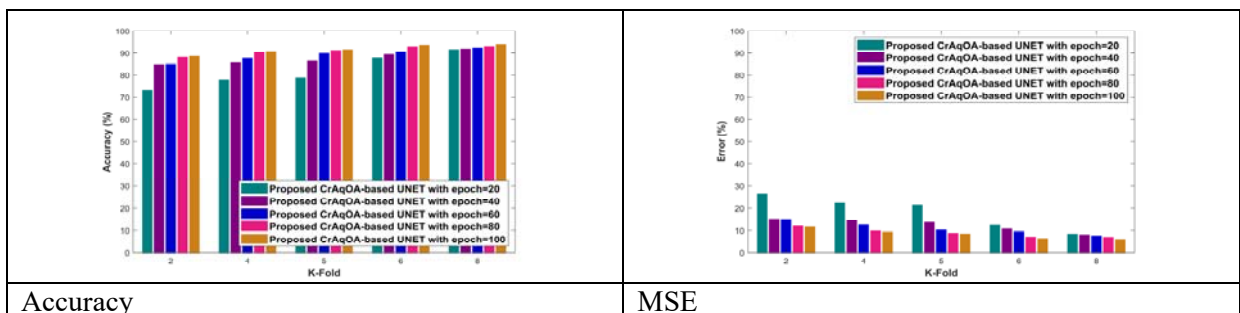


Figure 13. K-Fold Analysis of the projected model and existing models



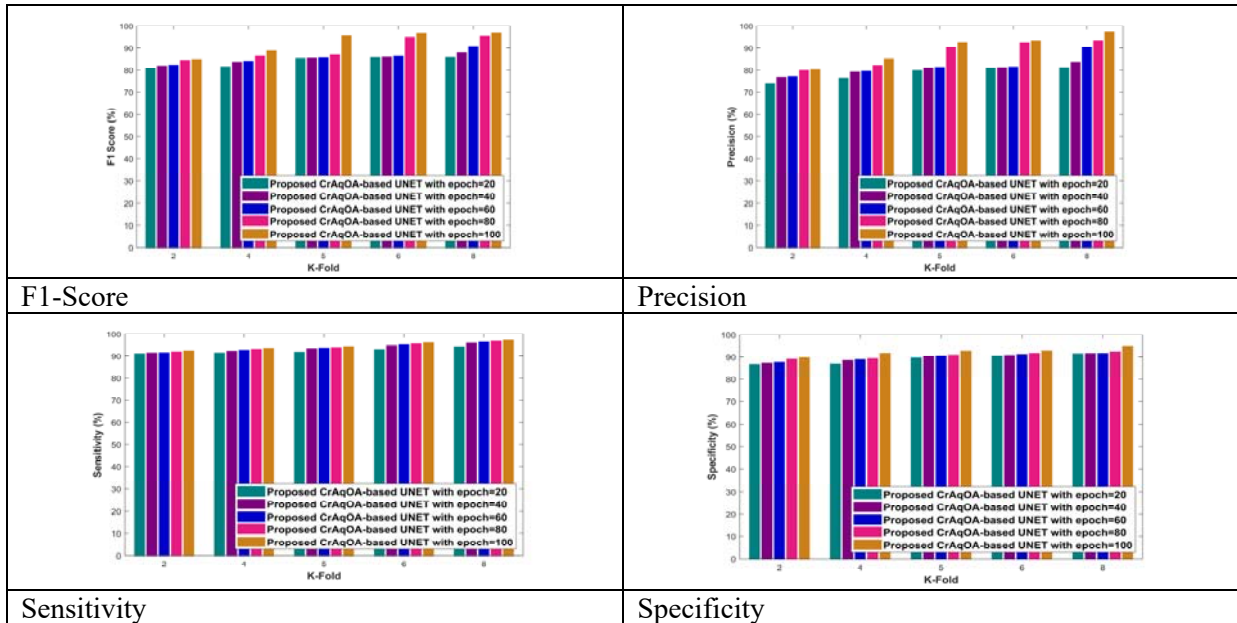


Figure 14. Performance Analysis of the projected model for varying epochs

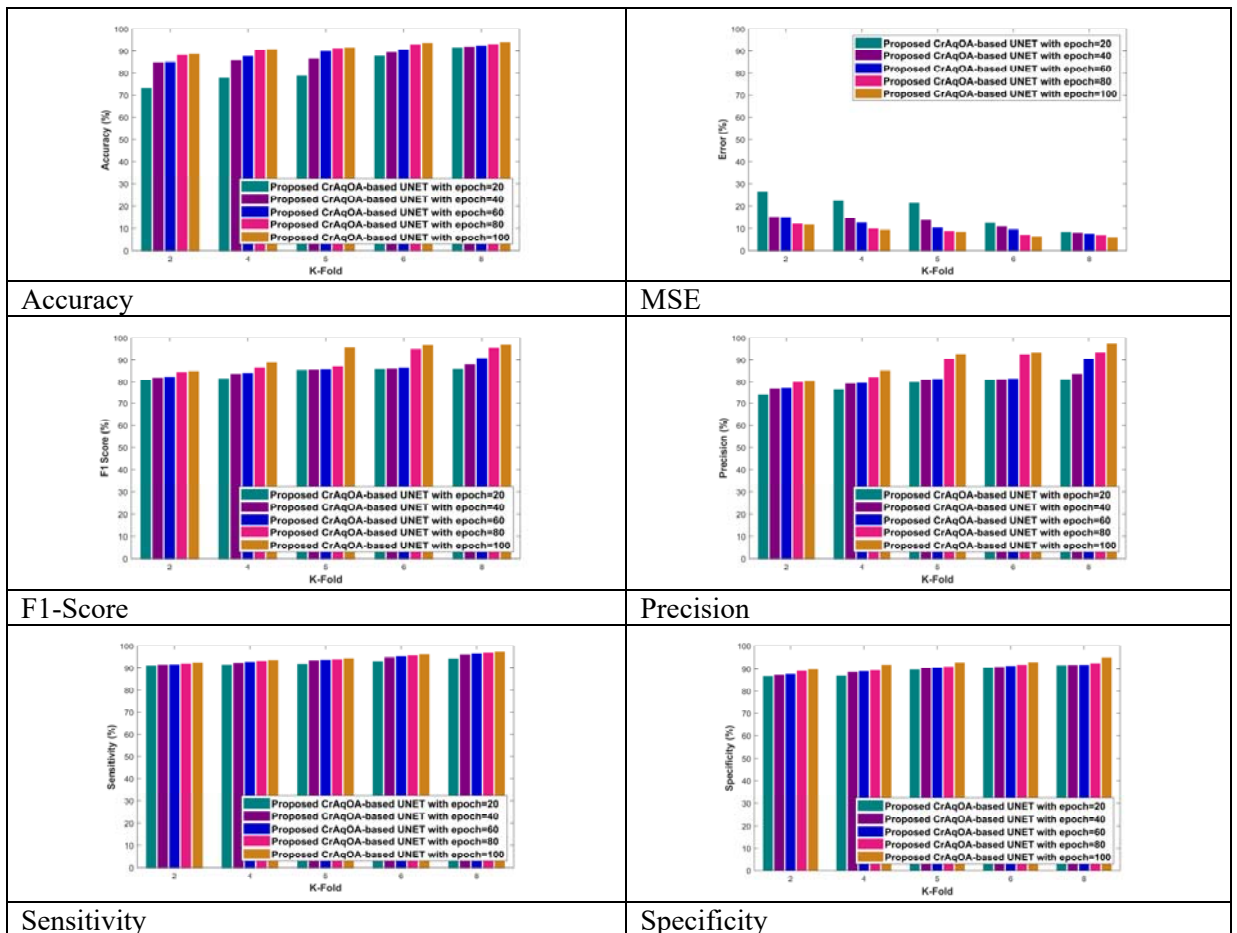


Figure 15. K-fold Analysis of the projected model for varying epochs

## 5. Conclusion

This research work has developed a new DCariesNet, a novel dental caries segmentation model. First, NRPMID, morphological procedures (dilation, erosion, opening, and closure), and histogram equalization were used to pre-process the dental X-ray images that had been obtained. From the pre-processed images, the three-fold features, such as LBP, LDP, and LOOP were retrieved. These recovered attributes are integrated to train the segmentation framework. A brand-new, enhanced U-NET-based CNN architecture has been employed to replicate the segmentation stage of dental caries. The weight function of U-NET has been optimized using an innovative CrAqOA. The CrAqOA model was developed by combining the conventional AO and conventional CSA ideas. The finalized outcome of the optimized U-NET is the segmented result (i.e. the region impacted by caries). Finally, a comparative study is performed to verify the efficacy of the predicted model. The evaluation takes into account accuracy, specificity, precision, sensitivity, F1-score, and MSE. At TP=90, the projected model's segmentation accuracy was 95.8%. This validates the efficacy of the proposed model over the conventional methods. In future, the ensemble model will be used to perform the segmentation process in such a way so as to improve the segmentation accuracy of the model.

## Conflict of Interest

The authors declare no conflict of interest.

## Author Contributions

Mohamed Shajahan Hussan Kannu carried out this research work under the supervision of TS. DR. SAHNIUS BT USMAN and PROF. TS. DR. NORLIZA MOHD NOOR. Mohamed Shajahan Hussan Kannu performed the experimental analysis for this prediction model. TS. DR. SAHNIUS BT USMAN, PROF. TS. DR. NORLIZA MOHD NOOR, TS. DR. SITI ARMIZA BINTI MOHD ARIS, and DR. RAMI NAHAS have provided critical feedback and helped shape the final version of the manuscript, and both the authors approved the final version of the manuscript.

## Acknowledgment

I wish to thank all my supervisors who provide their tremendous support in completing my research work. The continuous guidance of my committee members has made my research manuscript a successful project.

## References

- [1] Kumari, A. R., Rao, S. N., & Reddy, P. R. (2022). Design of hybrid dental caries segmentation and caries detection with meta-heuristic-based ResNet-RNN. *Biomedical Signal Processing and Control*, 78, 103961.
- [2] Ying, S., Wang, B., Zhu, H., Liu, W., & Huang, F. (2022). Caries segmentation on tooth X-ray images with a deep network. *Journal of Dentistry*, 119, 104076.
- [3] Zhu, Y., Xu, T., Peng, L., Cao, Y., Zhao, X., Li, S., ... & Liang, S. (2022). Faster-RCNN based intelligent detection and localization of dental caries. *Displays*, 74, 102201.
- [4] Leo, L. M., & Reddy, T. K. (2021). Learning compact and discriminative hybrid neural network for dental caries classification. *Microprocessors and Microsystems*, 82, 103836.
- [5] Zhao, Y., Li, P., Gao, C., Liu, Y., Chen, Q., Yang, F., & Meng, D. (2020). TSASNet: Tooth segmentation on dental panoramic X-ray images by Two-Stage Attention Segmentation Network. *Knowledge-Based Systems*, 206, 106338.
- [6] Lee, J. H., Kim, D. H., Jeong, S. N., & Choi, S. H. (2018). Detection and diagnosis of dental caries using a deep learning-based convolutional neural network algorithm. *Journal of dentistry*, 77, 106-111.
- [7] Li, S., Guo, Y., Pang, Z., Song, W., Hao, A., Xia, B., & Qin, H. (2022). Automatic Dental Plaque Segmentation Based on Local-to-Global Features Fused Self-Attention Network. *IEEE Journal of Biomedical and Health Informatics*, 26(5), 2240-2251.
- [8] Imak, A., Celebi, A., Siddique, K., Turkoglu, M., Sengur, A., & Salam, I. (2022). Dental caries detection using score-based multi-input deep convolutional neural network. *IEEE Access*, 10, 18320-18329.
- [9] Yu, H., Lin, Z., Liu, Y., Su, J., Chen, B., & Lu, G. (2020). A new technique for diagnosis of dental caries on the children's first permanent molar. *Ieee Access*, 8, 185776-185785.
- [10] Li, S., Guo, Y., Pang, Z., Song, W., Hao, A., Xia, B., & Qin, H. (2022). Automatic Dental Plaque Segmentation Based on Local-to-Global Features Fused Self-Attention Network. *IEEE Journal of Biomedical and Health Informatics*, 26(5), 2240-2251.
- [11] Lashgari, M., Shahmoradi, M., Rabbani, H., & Swain, M. (2018). Missing surface estimation based on modified tikhonov regularization: Application for destructed dental tissue. *IEEE Transactions on Image Processing*, 27(5), 2433-2446.
- [12] Thapa, D., Welch, R., Dabas, R. P., Salimi, M., Tavakolian, P., Sivagurunathan, K., ... & Tabatabaei, N. (2022). Comparison of long-wave and mid-wave infrared imaging modalities for photothermal coherence tomography of human teeth. *IEEE Transactions on Biomedical Engineering*, 69(9), 2755-2766.
- [13] Hyttinen, J., Fält, P., Jäsberg, H., Kullaa, A., & Hauta-Kasari, M. (2021). Computational Filters for Dental and Oral Lesion Visualization in Spectral Images. *IEEE Access*, 9, 145148-145160.
- [14] Resende Martins, J., B.Diaz-Fabregat, and C.Antoniali.2022.Salivary biomarkers of oxidative stress in children with dental caries: Systematic review and meta-analysis.*Archives of Oral Biology*.
- [15] Wang, Y., Zhang, Y., Pan, T., Lin, H., & Zhou, Y. (2022). Metabolic differences of the oral microbiome related to dental caries—A pilot study. *Archives of Oral Biology*, 141, 105471.
- [16] Yonezawa, D., & Yagi, M. (2022). Effect of a School-Based Fluoride Mouth-Rinsing Programme on Dental Caries. *international dental journal*, 72(4), 506-511.
- [17] Alazab, M., Islam, M., & Venkatraman, S. (2009). Towards automatic image segmentation using optimised region growing technique. In *AI 2009: Advances in Artificial Intelligence: 22nd Australasian Joint Conference, Melbourne, Australia, December 1-4, 2009. Proceedings 22* (pp. 131-139). Springer Berlin Heidelberg.

- [18] Hu, X., & Li, G. (2019). Temporal Tensor Local Binary Pattern: A Novel Local Tensor Time Series Descriptor. *IEEE Transactions on Industrial Informatics*, 16(10), 6393-6402.
- [19] Reddy, M. B., Sridhar, V., & Nagendra, M. (2012). Dental X-ray image analysis by using image processing techniques. *International Journal of Advanced Research in Computer Science and Software Engineering*, 2(6), 184-189.
- [20] Rad, A. E., Rahim, M. S. M., Kumoi, R., & Norouzi, A. (2012, January). Dental x-ray image segmentation and multiple feature extraction. In *2nd world conference on innovation and computer sciences* (Vol. 2, No. 2012, pp. 188-197).
- [21] Rad, A. E., Rahim, M. S. M., & Norouzi, A. (2013). Digital dental X-ray image segmentation and feature extraction. *TELKOMNIKA Indonesian Journal of Electrical Engineering*, 11(6), 3109-3114.
- [22] Rad, A. E., Amin, I. B. M., Rahim, M. S. M., & Kolivand, H. (2015). Computer-aided dental caries detection system from X-ray images. In *Computational Intelligence in Information Systems: Proceedings of the Fourth INNS Symposia Series on Computational Intelligence in Information Systems (INNS-CIIS 2014)* (pp. 233-243). Springer International Publishing.
- [23] Rad, A. E., Rahim, M. S. M., Kolivand, H., & Norouzi, A. (2018). Automatic computer-aided caries detection from dental x-ray images using intelligent level set. *Multimedia Tools and Applications*, 77, 28843-28862.
- [24] Panyarak, W., Wantanajittikul, K., Suttapak, W., Charuakkra, A., & Prapayasatok, S. (2023). Feasibility of deep learning for dental caries classification in bitewing radiographs based on the ICCMS™ radiographic scoring system. *Oral Surgery, Oral Medicine, Oral Pathology and Oral Radiology*, 135(2), 272-281.
- [25] Besnard, C., Marie, A., Buček, P., Sasidharan, S., Harper, R. A., Marathe, S., ... & Korsunsky, A. M. (2022). Hierarchical 2D to 3D micro/nano-histology of human dental caries lesions using light, X-ray and electron microscopy. *Materials & Design*, 220, 110829.
- [26] Bayrakdar, I. S., Orhan, K., Akarsu, S., Çelik, Ö., Atasoy, S., Pekince, A., ... & Odabaş, A. (2021). Deep-learning approach for caries detection and segmentation on dental bitewing radiographs. *Oral Radiology*, 1-12.
- [27] Hyttinen, J., Fält, P., Jäsberg, H., Kullaa, A., & Hauta-Kasari, M. (2021). Computational Filters for Dental and Oral Lesion Visualization in Spectral Images. *IEEE Access*, 9, 145148-145160.
- [28] Zhu, H., Cao, Z., Lian, L., Ye, G., Gao, H., & Wu, J. (2022). CariesNet: a deep learning approach for segmentation of multi-stage caries lesion from oral panoramic X-ray image. *Neural Computing and Applications*, 1-9.
- [29] Choi, J., Eun, H., & Kim, C. (2018). Boosting proximal dental caries detection via combination of variational methods and convolutional neural network. *Journal of Signal Processing Systems*, 90, 87-97.
- [30] Singh, P., & Sehgal, P. (2021). GV Black dental caries classification and preparation technique using optimal CNN-LSTM classifier. *Multimedia Tools and Applications*, 80, 5255-5272.
- [31] Datta, S., Chaki, N., & Modak, B. (2020). Neutrosophic set-based caries lesion detection method to avoid perception error. *SN Computer Science*, 1, 1-15.
- [32] Park, G. H., Cho, H. H., & Choi, M. R. (2008). A contrast enhancement method using dynamic range separate histogram equalization. *IEEE Transactions on Consumer Electronics*, 54(4), 1981-1987.
- [33] Martins, J. R., Díaz-Fabregat, B., Ramirez-Carmona, W., Monteiro, D. R., Pessan, J. P., & Antoniali, C. (2022). Salivary biomarkers of oxidative stress in children with dental caries: Systematic review and meta-analysis. *Archives of Oral Biology*, 139, 105432.
- [34] Karthika Devi, R., Banumathi, A., & Ulaganathan, G. (2019). An automated and hybrid method for cyst segmentation in dental x-ray images. *Cluster Computing*, 22, 12179-12191.
- [35] Kumar, A., Bhadauria, H. S., & Singh, A. (2020). Semi-supervised OTSU based hyperbolic tangent Gaussian kernel fuzzy C-mean clustering for dental radiographs segmentation. *Multimedia Tools and Applications*, 79, 2745-2768.
- [36] Nishitani, Y., Nakayama, R., Hayashi, D., Hizukuri, A., & Murata, K. (2021). Segmentation of teeth in panoramic dental X-ray images using U-Net with a loss function weighted on the tooth edge. *Radiological Physics and Technology*, 14, 64-69.
- [37] Qaddoura, R., Manaseer, W. A., Abushariah, M. A., & Alshraideh, M. A. (2020). Dental radiography segmentation using expectation-maximization clustering and grasshopper optimizer. *Multimedia Tools and Applications*, 79, 22027-22045.
- [38] Solanki, A., Jain, K., & Desai, N. (2013). Isef based identification of rct/filling in dental caries of decayed tooth. *International Journal Image Processing (IJIP)*, 7(2), 149-162.
- [39] SHARMILA.M, Dr.R.GANESAN, and R.KARTHIKA DEVI.2013.Detection of Dental Plaque using Image Processing.*International Journal of Advanced Information Science and Technology (IJAIIST)* ISSN: 2319:2682 .18(18).
- [40] Krithiga, R. R., Lakshmi, C., & Nithya, A. A. (2014). Segmentation of dental caries from dental X-ray images using wavelet and watershed transforms. *International Journal of Applied Engineering Research*, 9(20), 2014.
- [41] Kaushik, A., Mathpal, P. C., & Sharma, V. (2014). Edge detection and level set active contour model for the segmentation of cavity present in dental X-ray images. *International Journal of Computer Applications*, 96(9).
- [42] NarainPonraj, D., Christy, E., Aneesha, G., Susmitha, G., & Sharu, M. (2018, March). Analysis of LBP and LOOP based textural feature extraction for the classification of CT Lung images. In *2018 4th International Conference on Devices, Circuits and Systems (ICDCS)* (pp. 309-312). IEEE.
- [43] Jeon, K. M., Chun, C., Kim, G., Leem, C., Kim, B., & Choi, W. (2020, January). Lightweight U-Net Based Monaural Speech Source Separation for Edge Computing Device. In *2020 IEEE International Conference on Consumer Electronics (ICCE)* (pp. 1-4). IEEE.
- [44] Hussien, A. G., Amin, M., Wang, M., Liang, G., Alsanad, A., Gumaei, A., & Chen, H. (2020). Crow search algorithm: theory, recent advances, and applications. *IEEE Access*, 8, 173548-173565.
- [45] Abualigah, L., Yousri, D., Abd Elaziz, M., Ewees, A. A., Al-Qaness, M. A., & Gandomi, A. H. (2021). Aquila optimizer: a novel meta-heuristic optimization algorithm. *Computers & Industrial Engineering*, 157, 107250.
- [46] Doddawad, V. G., Shivananda, S., Paul, N. J., & Chandrakala, J. (2022). Dental caries: Impact of tobacco product among tobacco chewers and tobacco smokers. *Journal of Oral Biology and Craniofacial Research*, 12(3), 401-404.
- [47] Hassan, H. A., Tahir, N. M., Yassin, I., Zabidi, A., Yahaya, C. H. C., & Shafie, S. M. (2013, December). Automated optic disc removal in fundus images using iterative heuristics and morphological operations. In *2013 IEEE Conference on Systems, Process & Control (ICSPC)* (pp. 230-233). IEEE.
- [48] Geetha, V., K.S.Aprameya , and D.M.Hinduja .2022.Dental caries diagnosis in digital radiographs using back-propagation neural network.*Health Information Science and Systems*
- [49] Jabid, T., Kabir, M. H., & Chae, O. (2010, January). Local directional pattern (LDP) for face recognition. In *2010 digest of technical papers international conference on consumer electronics (ICCE)* (pp. 329-330). IEEE.

### Author's Profile



**Mohamed Shajahan** is from India. He received the B.Sc degree in Computer Science and M.Sc in Computer Science from Manonmanium Sundaranar University, India. He is currently pursuing his Ph.D since 2019 from Universiti Teknologi Malaysia, Kuala Lumpur. He is currently a senior lecturer at College of Engineering, University of Business and Technology, Jeddah, Saudi Arabia. His current research interests are Image Processing, data mining, and machine learning.



**Sahnus Usman** was received the B. Eng. degree in Mechatronic Engineering and MEE (Electrical) from Universiti Teknologi Malaysia (UTM) and PhD degree in Electrical & Electronic Engineering from Universiti Kebangsaan Malaysia (UKM), in 1999, 2003 and 2015 respectively. She is currently a lecturer in Universiti Teknologi Malaysia, Kuala Lumpur. She is currently involved with research work related with biomedical engineering, artificial intelligence and blockchain.



**Siti Armiza** (Senior Member, IEEE) is from Kuala Lumpur, Malaysia. She received the B.Eng degree in Electrical Engineering (Microelectronics) and M.Eng in Electrical Engineering from Universiti Teknologi Malaysia in 1998 and 2001 respectively. She obtained her Ph.D. in Electrical Engineering (Biomedical) from Universiti Teknologi MARA in 2016. She is currently a senior lecturer at Razak Faculty of Technology and Informatics, UTM Kuala Lumpur. Her current research interests include but not limited to EEG signal processing, bio-signal processing, psycho-physiological interactive tools, and bio-signal monitoring tools, data mining, and machine learning. She is a senior member of IEEE Malaysia Section, IEEE EMBS Malaysia Society, IEEE Signal Processing Society Malaysia Chapter, and IEEE KL Subsection. In 2016, her research paper has been recognized by the IEEE WIE and awarded as the best research paper for her outstanding work.



**NORLIZA MOHD NOOR** (FAPM - Fellow, Akademi Professor Malaysia, SMIEEE – Senior Member IEEE) received the B.Sc. degree in electrical/electronic engineering from Texas Tech University, Lubbock, TX, USA, and the master's degree in electrical engineering (by research) and the Ph.D. degree in electrical engineering (signal processing) from Universiti Teknologi Malaysia. She is currently a Professor at the Razak Faculty of Technology and Informatics, UTM, Kuala Lumpur Campus. Her research interests include image analysis and machine learning.